bioRxiv preprint doi: https://doi.org/10.1101/2020.10.27.357673; this version posted October 27, 2020. The copyright holder for this preprint (which was not certified by peer review) is the author/funder. All rights reserved. No reuse allowed without permission.

Transcriptome and Chromatin Landscape of iNKT cells are Shaped by Subset Differentiation and Antigen Exposure

(21/130)

Mallory Paynich Murray[1#], Isaac Engel[1#], Gregory Seumois[1#], Sara Herrera de la Mata[1], Sandy Lucette Rosales[1], Ashu Sethi[1], Ashmitaa Logandha Ramamoorthy Premlal[1], Goo-Young Seo[1], Jason Greenbaum[1], Pandurangan Vijayanand[1,2,3], and James P. Scott-Browne[1,4*] and Mitchell Kronenberg[1,5*]

[#]Co-first authors

[*]Co-Corresponding authors

Affiliations:

1 La Jolla Institute for Immunology, La Jolla, CA, USA

2 University of Southampton, Faculty of Medicine, Southampton, UK

3 Department of Medicine, University of California San Diego, La Jolla, CA, USA

4 Department of Biomedical Research, National Jewish Health, Denver, CO, USA

5 Division of Biological Sciences, University of California San Diego, La Jolla, CA, USA

bioRxiv preprint doi: https://doi.org/10.1101/2020.10.27.357673; this version posted October 27, 2020. The copyright holder for this preprint (which was not certified by peer review) is the author/funder. All rights reserved. No reuse allowed without permission.

Abstract

Invariant natural killer T cells (iNKT cells) differentiate into thymic and peripheral NKT1, NKT2 and NKT17 subsets. We determined if the gene programs associated with these thymic subsets were maintained in peripheral sites, the influence of tissue location, and if there were large-scale changes after antigen exposure. RNA-seq and ATAC-seq analyses showed that iNKT cells in any subset were similar, regardless of tissue location. Lung iNKT cell subsets possessed the most distinct location-specific features, shared with other innate lymphocytes in the lung, possibly consistent with increased activation. After antigenic stimulation, iNKT cells underwent chromatin and transcription changes leading to two populations: one similar to follicular helper T cells and the other like NK or effector cells. Phenotypic analysis indicated these changes were observed long-term, suggesting that iNKT cells gene programs are not fixed, but they are capable of chromatin remodeling after antigen to give rise to several new subsets.

bioRxiv preprint doi: https://doi.org/10.1101/2020.10.27.357673; this version posted October 27, 2020. The copyright holder for this preprint (which was not certified by peer review) is the author/funder. All rights reserved. No reuse allowed without permission.

Introduction

Invariant Natural Killer T (iNKT) cells are considered to be an innate-like T lymphocyte population that can initiate or inhibit immune responses, depending on the context. Following activation, iNKT cells rapidly produce copious amounts of cytokines, similar to other innate-like lymphocytes[1]. iNKT cells express an invariant TCRα chain comprised of a Vα14-Jα18 (*Trav11-Traj18*) rearrangement in mice, with a conserved rearrangement in humans and many other mammals. These cells are activated by either self or microbial glycolipid antigens, presented by CD1d, a non-classical MHC class I molecule[2].

In the thymus, iNKT cells differentiate into three effector cell subsets, NKT1, NKT2, and NKT17, without exposure to exogenous antigen. Their effector functions and cytokine profiles resemble T_H1, T_H2, and T_{H17} $CD4^+$ T cells and subsets of other lymphocytes, including ILC, mucosal associated invariant T (MAIT) cells and γδ T cells[3, 4, 5]. Within the thymus, these iNKT cell subsets have highly divergent epigenetic landscapes and transcriptional programs[6, 7, 8]. Remarkably, several hundred genes are differentially expressed between thymic iNKT cell subsets, despite their similar specificity and despite sharing a distinct positive selection pathway[9]. Evidence suggests that some iNKT cells are long-term thymic residents, and these resident cells may contribute to thymic homeostasis[6]. Following egress from the thymus, iNKT cells localize to tissues throughout the body and the majority of peripheral iNKT cells do not recirculate[10, 11].

Although divergent thymic iNKT cell subsets have been identified, their relationship to

bioRxiv preprint doi: https://doi.org/10.1101/2020.10.27.357673; this version posted October 27, 2020. The copyright holder for this preprint (which was not certified by peer review) is the author/funder. All rights reserved. No reuse allowed without permission.

65 the corresponding peripheral iNKT cell subsets has not been assessed. Also, the
66 impact of tissue localization on gene expression programs remains incompletely
67 understood. To address these issues, we compared transcriptomic and epigenomic
68 data of iNKT cells from the thymus to several peripheral sites. Similar methods were
69 used to track changes in these cells after antigen exposure. Our genome-wide analysis
70 of the transcriptome and epigenome of iNKT cell subsets provides insights into the
71 stability and plasticity of the chromatin landscapes that are potentially initiated in the
72 thymus.
73
74

bioRxiv preprint doi: https://doi.org/10.1101/2020.10.27.357673; this version posted October 27, 2020. The copyright holder for this preprint (which was not certified by peer review) is the author/funder. All rights reserved. No reuse allowed without permission.

Results

Divergent chromatin landscape of thymic iNKT cell subsets

Previously, we showed that thymic iNKT cell subsets possess highly divergent transcriptomes[8]. Similar results were obtained by others[7, 11, 12]. Further, we demonstrated by genome-wide analysis of H3K27 acetylation modification that there were significant differences in enhancer marks between the thymic iNKT cell subsets[8]. Because the epigenetic landscape of a cell population is more stable than the transcriptome, we analyzed the epigenetic landscape of thymic iNKT cell subsets more broadly with the assay for transposase-accessible chromatin using sequencing (ATAC-seq)[13]. The thymic iNKT cell subsets were sorted based on expression of surface proteins and validated by transcription factor staining (Supplementary Fig. 1a, 1b). Based on our previous RNA-seq analysis of thymic iNKT cell subsets, we excluded a population of CD1d-tetramer^{+} cells with an intermediate phenotype, ICOS^{high} or IL17RB^{+} cells that express CXCR3 or CD122, to obtain more purified subsets (Supplementary Fig. 1c). Expression of *Rorc* and *Tbx21* transcripts by each iNKT cell subset in multiple tissue tissues further demonstrates sorting efficiency; *Rorc* transcripts are only expressed in NKT17 cells, whereas *Tbx21* transcripts are predominately expressed in NKT1 cells (Supplementary Fig. 1d).

Consistent with previous results, we found that the profiles of accessible chromatin in iNKT cell thymic subsets were strikingly divergent, with between approximately 5,000-7,500 differentially accessible regions of chromatin (Fig. 1a). For comparison, naïve

bioRxiv preprint doi: https://doi.org/10.1101/2020.10.27.357673; this version posted October 27, 2020. The copyright holder for this preprint (which was not certified by peer review) is the author/funder. All rights reserved. No reuse allowed without permission.

versus memory CD8$^+$ T cells have approximately 5,700 differentially accessible regions of chromatin[14, 15]. Fig. 1b highlights the results from some key cytokine and transcription factor gene loci. For example, there was a higher ATAC-seq signal at the *Ifng* locus in thymic in NKT1 cells (Fig. 1b). Although some signal at several peaks also was apparent in NKT2 cells, no accessibility was detected at a proximal enhancer 5 kb upstream of the TSS (vertical grey bar) required for *Ifng* transcription (Fig. 1b)[16]. As expected, we found the *Il17a* locus was most accessible in NKT17 cells. The *Il4* and *Il13* loci were open in both NKT2 and NKT1 cells, likely reflecting the ability of NKT1 cells to produce some Th2 cytokines after strong activation (Fig. 1b). Similarly, for transcription factors that drive the expression of key cytokines, the *Tbx21* locus encoding T-bet was more accessible in NKT1 cells and accessibility of *Rorc* was increased in NKT17 cells (Fig. 1b, right). *Zbtb16* encoding PLZF, a transcription factor required for the generation of all iNKT cells[9], was accessible in all subsets, although mRNA and protein expression (Supplementary Fig. 1b) were higher in NKT2 thymocytes.

We partitioned all differentially accessible regions between thymic subsets (Fig. 1a) into eight groups with *k*-means clustering to identify potential regulatory elements with similar changes in ATAC-seq signal. We then examined the degree to which the regions in each group were accessible in the different thymocyte iNKT cell subsets (Fig. 1c). Regions in clusters 1-3 had the highest signal in NKT1 cells, while clusters 4-5 and 6-8 had the highest signal in NKT2 and NKT17 cells, respectively. To associate the changes in regulatory element accessibility with transcription factors, we determined the

bioRxiv preprint doi: https://doi.org/10.1101/2020.10.27.357673; this version posted October 27, 2020. The copyright holder for this preprint (which was not certified by peer review) is the author/funder. All rights reserved. No reuse allowed without permission.

enrichment of known motifs associated with DNA binding proteins. Within clusters 1-3, typical of NKT1 cells, accessible regions frequently contained Tbox motifs, and to a lesser extent Runt and Et1 motifs. HMG box protein motifs, associated with Tcf1 and Lef1, were enriched in NKT2 thymocytes along with some enrichment for zinc finger and RHD domain motifs, which include Egr1 and Nfat motifs, respectively. Expression of Tcf1 (encoded by *Tcf7*) is enriched in NKT2 cells and required for iNKT cell development[17]. Additionally, Lef1 is required for iNKT cell expansion and NKT differentiation, independent of Tcf1[18]. Regions accessible in NKT17 cells were enriched for consensus motifs of nuclear receptors, which can include Rorc and Reverb (Fig. 1d).

iNKT cell subsets in different sites are similar

To understand the degree to which the gene programs associated with thymic subsets were also present in the periphery, and to assess the impact of tissue localization on chromatin accessibility and the transcriptome, we compared sorted iNKT cell subsets from thymus to those in spleen, liver and lung by both RNA-seq and ATAC-seq analysis. Previous work showed that NKT1 cells were the predominant iNKT cell population in C57BL/6J mice, comprising the majority in all the tissue sites analyzed[6]. NKT17 cells preferentially localized to the lung, lymph nodes and skin, and NKT2 cells were more abundant in the spleen and mesenteric lymph nodes[6]. Because of the very low cell numbers, NKT2 and NKT17 cells from liver were not analyzed. Although we used a different RNA-seq technology allowing for greater sequencing depth[19], we found exceedingly similar gene expression profiles in thymic NKT1, NKT2 and NKT17 thymocytes compared to the previous study[8] (Supplementary Fig. 2). Based on bulk

bioRxiv preprint doi: https://doi.org/10.1101/2020.10.27.357673; this version posted October 27, 2020. The copyright holder for this preprint (which was not certified by peer review) is the author/funder. All rights reserved. No reuse allowed without permission.

RNA-seq analysis, we observed that, as in the thymus, iNKT cell subsets within a given tissue were distinct from one another (Supplementary Fig. 2). Similarly, the chromatin accessibility profiles of iNKT subsets from spleen showed a divergent pattern of accessible regions (Fig. 2a). Although splenic NKT2 and NKT17 cells were more similar to one another than their thymic counterparts, there remained more than 3,500 differentially accessible loci (Fig. 2a).

In comparing thymic iNKT cell subsets with their peripheral counterparts, we found smaller differences related to the tissue location compared to differences that were associated with the subset identity. For example, comparing peripheral NKT1 to thymic NKT1 cells, we found less than 1,000 differentially accessible chromatin regions (data not shown). Similarly, we observed relatively few differences in accessible chromatin regions comparing NKT1 cells between different peripheral tissues (Fig. 2b). Similar results were obtained from analyzing chromatin accessibility in NKT2 and NKT17 cells from different tissues. Principal component analyses (PCA) of the ATAC-seq data revealed the strong influence of subset identity (Fig. 2c). A similar conclusion was obtained for the RNA-seq data, although we did find some separation based on tissue (Fig. 2d). These data are consistent with a model in which the chromatin accessibility patterns set up for iNKT cells in the thymus largely carry over into the periphery, where iNKT cell subset transcriptomes exhibit a high degree of similarity to thymic counterparts.

bioRxiv preprint doi: https://doi.org/10.1101/2020.10.27.357673; this version posted October 27, 2020. The copyright holder for this preprint (which was not certified by peer review) is the author/funder. All rights reserved. No reuse allowed without permission.

Despite the overall similarity between the thymus and peripheral tissues, there are transcripts that were enriched specifically in a given thymic subset compared to the same subset in each peripheral site, including *Egr2* and *Tox* (Fig. 2e). These transcription factors are required for the early stages of iNKT cell differentiation[20, 21], so-called NKT0 cells, and therefore this may reflect residual expression of these genes in mature thymic iNKT cell subsets, long-lived in the thymus. Some transcripts were the converse, enriched in all or several peripheral tissues compared to thymus, without subset restriction. These include *Art2* and *P2rx7*, previously reported to be increased in total populations of peripheral iNKT cells[22], which make cells sensitive to NAD-induced cell death, and *Osgin1*, identified as a growth inhibitory protein in other contexts[23]. The expression of these genes might reflect the need for brakes on the expansion and function of potentially autoreactive iNKT cells[24]. Also enriched in all sites in peripheral iNKT cells were *Tspan13*, and *Klf3*, whose expression was increased in memory $CD8^+$ T cells[25].

Identification of a gene expression signature in lung

Although the iNKT cell subset is a predominant factor driving genomic differences, lung iNKT cells shared common features that distinguished them from their counterparts in the other locations. This was revealed by PC2 of the RNA-seq data (Fig. 2d), or PC3 analysis of the ATAC-seq data (Fig. 3a). Transcripts encoding AP-1 and other bZIP family members, as well as some members of the NF-κB family were enriched in all lung iNKT cell subsets, as were transcripts encoding CTLA-4, CD69 and *Nr4a1* encoding Nur77 (Fig. 3b and Supplementary Fig. 3). Furthermore, regions more

bioRxiv preprint doi: https://doi.org/10.1101/2020.10.27.357673; this version posted October 27, 2020. The copyright holder for this preprint (which was not certified by peer review) is the author/funder. All rights reserved. No reuse allowed without permission.

accessible in lung iNKT cells were enriched for bZIP motifs, which are associated with the transcription factors Ap1 and Atf, as well as RHD motifs, which can include NFκB-p65 binding sites (Fig. 3c). Together these data are consistent with tissue-residency or increased activation of lung iNKT cells, and indeed, we found a subpopulation of lung iNKT cells that expressed CTLA-4 by flow cytometry (Fig. 3d). To ascertain that the signature in lung iNKT cells could not be attributed to infection or inflammation in a single mouse, we sorted iNKT cell subsets from individual mice obtained only one week earlier from a commercial supplier and performed RNA-seq. We found a similar lung gene expression signature in each individual (Supplementary Fig. 3).

Cells within the lung are exposed to a diverse environment of environmental and microbial antigens, as well as differences in oxygen. We next asked if iNKT cells from another antigen-rich site, the small intestine, displayed a similar increase in CTLA-4 expression. We found that total iNKT cells from the small intestinal lamina propria (SI-LPL) express CTLA-4 similarly to lung iNKT cells, whereas splenic iNKT cells do not (Fig. 3e). These data suggest antigen-rich environments may imprint the lung activation signature.

Other innate or innate-like lymphocyte populations are found in lung, including γδ T cells, MAIT cells, ILC and NK cells, as well as mainstream resident lymphocytes and some circulating cells. We tested if the lung activation signature of iNKT cells extended to several other lung populations. Therefore, we performed ATAC-seq and RNA-seq analyses on sorted γδ T cells, NK cells, as well as naïve $CD4^+$ T cells from the lung and

bioRxiv preprint doi: https://doi.org/10.1101/2020.10.27.357673; this version posted October 27, 2020. The copyright holder for this preprint (which was not certified by peer review) is the author/funder. All rights reserved. No reuse allowed without permission.

spleen. Lung γδ T cells and NK cells displayed the lung signature based on increased chromatin accessibility in regions enriched for bZIP and RHD motifs (Fig. 4a), with γδ T cells having accessibility in regions enriched for nuclear receptor motifs, which can include RORγt binding sites, while NK cells were enriched for T-box motifs. Lung $CD4^+$ T cells had a different pattern from the other cell types, but with some increased signal at regions containing bZIP (ATF) and RHD (NF-κB-p65) motifs (Fig. 4a). PCA analysis of the RNA-seq data, which included total iNKT cells from spleen or lung, showed separation of each lung cell type, including $CD4^+$ T cells, from the corresponding cell type in spleen (Fig. 4b). Further, we found increased expression of the iNKT cell lung signature genes, listed in Supplementary Fig. 3, in lung γδ T cells, and NK cells compared to the corresponding splenic populations (Fig. 4c). The transcriptome of lung $CD4^+$ T cells was more divergent, but still had some features in common with the lung-resident innate or innate-like lymphocyte populations (Fig. 4c). This is illustrated in Fig. 4d, which shows that expression of *Fosl2, Bhlhe40* and *Tnfaip3* was higher in all cell types from the lung. Gene set enrichment analysis (GSEA) pre-ranked analysis comparing each cell type from the lung versus spleen using the iNKT cell lung signature further demonstrated the strong enrichment of the lung signature in each cell type (Fig. 4e).

Epigenomic and transcriptomic changes following antigen challenge

A unifying hypothesis based on these data is that iNKT cell subsets are formed in the thymus and seed peripheral tissues with fixed functions and relatively minor impacts to their chromatin landscape and transcriptomic profiles, with the partial exception of those

bioRxiv preprint doi: https://doi.org/10.1101/2020.10.27.357673; this version posted October 27, 2020. The copyright holder for this preprint (which was not certified by peer review) is the author/funder. All rights reserved. No reuse allowed without permission.

in the lung. To test this, we determined if these profiles remained after a strong antigenic challenge in total splenic iNKT cells, which are mostly NKT1 cells. To examine how the chromatin landscape and transcriptome of iNKT cells was altered in response to antigen, we injected mice with αGalCer and harvested the spleen 6 days later. It has been reported that following exposure to the potent glycolipid antigen α-galactosyl ceramide (αGalCer), some iNKT cells display a T follicular helper cell (T_{FH})-like phenotype, with increased expression of CXCR5, PD-1, and BCL6 (Supplementary Fig. 4a, 4b). These so-called NKT_{FH} cells produce IL-21, and localize to germinal centers[26], and may play a role in early germinal center formation[27], but their gene expression programs had not been elucidated. Putative NKT_{FH} (αGalCer loaded CD1d tetramer$^+$CXCR5$^+$PD-1$^+$) and the remaining population of iNKT cells from antigen-injected mice (CXCR5$^-$PD-1$^-$ or NKT non-FH) cells were sorted and analyzed by ATAC-seq and RNA-seq. Of note, NKT1, NKT2 and NKT17 cells as described above are not identifiable 6 days following αGalCer challenge and therefore were not analyzed. As shown in Fig. 5a, accessible regions of chromatin were exceptionally different comparing NKT_{FH} and the antigen-exposed non-FH cells, which we refer to as iNKT cell effectors (NKT_{eff}). Chromatin accessibility regions in NKT_{FH} were also very different from the NKT1, NKT2 and NKT17 subsets in the spleen from uninjected mice, most different from NKT17 cells (Fig. 5a, left). There was increased chromatin accessibility in NKT_{FH} in the *Il21* locus and the *Pdcd1* locus encoding PD-1 in NKT_{FH} cells (Fig. 5b), reflecting a T_{FH} state. The accessible regions of chromatin within NKT_{eff} also greatly varied when compared to the iNKT cell subsets from unchallenged mice but were most

bioRxiv preprint doi: https://doi.org/10.1101/2020.10.27.357673; this version posted October 27, 2020. The copyright holder for this preprint (which was not certified by peer review) is the author/funder. All rights reserved. No reuse allowed without permission.

similar to NKT1 cells (Fig. 5a, right). These data suggest that most of the splenic iNKT cells were exposed to antigen, including those that did not become NKT_{FH}.

We partitioned all differentially accessible regions between NKT_{FH} and NKT_{eff} cells and splenic iNKT cell subsets from unimmunized mice into ten groups with *k*-means clustering to identify regions with similar changes in ATAC-seq signal. As above, we examined the degree to which the regions in each group were differentially accessible in iNKT cell populations (Fig. 5c) and their association with DNA binding protein motifs (Fig. 5c). Notably, the two populations from αGalCer immunized mice had increased accessibility for cluster 7, with motifs for T-box proteins and to a lesser extent NFκB (RHD motifs) and IRF proteins. There also was decreased accessibility in regions containing motifs associated with the lineage driving transcription factors RORγt (nuclear receptor motifs) and GATA3 (zinc finger motifs) enriched in clusters 1 and 2. Accessible regions specific to NKT_{FH} cells within clusters 8 and 9 were increased for motifs for RHD domain transcription factors, which include NFAT and NFκB, and bZIP motifs, characteristic of Ap-1 family transcription factors, suggesting a more activated state. Clusters 4 and 5 were more accessible in NKT_{eff} and also in NKT1 cells from unimmunized mice. These accessible regions were enriched for T-bet, Ets and Runt domain-associated motifs. NKT_{eff} cells also had increased accessibility in regions containing more Zinc finger transcription factor and Ets motifs (cluster 6). Although they are reported to be self-reactive, these data suggest that iNKT cells greatly remodel their chromatin landscape following encounter with a potent exogenous glycolipid antigen.

bioRxiv preprint doi: https://doi.org/10.1101/2020.10.27.357673; this version posted October 27, 2020. The copyright holder for this preprint (which was not certified by peer review) is the author/funder. All rights reserved. No reuse allowed without permission.

We also performed RNA-seq on the two populations of iNKT cells from αGalCer-treated mice, as well as total splenic iNKT cells from unimmunized mice. Gene expression by NKT_{FH} was greatly different from total splenic iNKT cells (Fig. 5d) or from each of the iNKT cell subsets from unchallenged mice (Fig. 5e, Supplementary Fig. 4c). Comparison of differentially expressed genes distinguishing $CD4^+$ T_{FH} and T_H1 cells[28] demonstrated that NKT_{FH} shared a more similar expression profile to T_{FH}, whereas, not surprisingly, NKT1 cells were similar to T_H1 (Supplementary Fig. 4d). Similarities between NKT_{FH} and T_{FH} also were revealed by GSEA analysis (Fig. 5f, top panel). GSEA of NKT_{FH} compared to NKT_{eff} revealed an enrichment for $CD8^+$ T cell effector-related genes in NKT_{eff} (Fig. 5f, bottom, left and right panels). Neither antigen-experienced subset was significantly enriched for memory cell-related signatures.

Because of the great prevalence of NKT1 cells in the spleens of unimmunized C57BL/6J mice[6], it was not feasible to assess directly the separate contributions of the NKT1, NKT2 and NKT17 subsets to the antigen-activated iNKT cell populations. To address their origin, we utilized mice in which T-bet expression could be fate-mapped[29]. Whereas close to 90% of spleen NKT1 cells from unimmunized mice expressed the T-bet fate map marker, only 74% or less of NKT_{FH} did (Fig. 5g). Notably, the T-bet fate map marker was not expressed in NKT2 cells. Therefore, some NKT_{FH} may have originated from the prevalent NKT1 cell pool, and despite their separation from NKT1 cells, we found expression of some NKT1 signature genes by NKT_{FH} (Supplementary Fig. 4d). However, because prior T-bet expression was selected against in NKT_{FH} cells, these data suggest that NKT2 and/or NKT17 cells also may have contributed.

bioRxiv preprint doi: https://doi.org/10.1101/2020.10.27.357673; this version posted October 27, 2020. The copyright holder for this preprint (which was not certified by peer review) is the author/funder. All rights reserved. No reuse allowed without permission.

Furthermore, the fate-mapping may underestimate how efficiently NKT2 and/or NKT17 converted to NKT_{FH}; T-bet expression could have been induced in some iNKT cells after antigen activation.

Enhanced effector function after antigen challenge

As shown in Fig. 5a (right column), iNKT cells from αGalCer-immunized mice that did not become NKT_{FH} also had a chromatin landscape different from all of the subsets in unimmunized mice, with the biggest divergence again from NKT17 cells. PCA analysis of the RNA-seq data showed that the transcriptome of these iNKT cells was highly different from total iNKT cells from unimmunized mice (Fig. 5d). Previous analyses have shown that after i.v. exposure to DCs loaded with αGalCer, a $KLRG1^+$ population of iNKT cells develops, especially in the lung, in a process dependent on expression of the transcription factor Eomes[30, 31]. Cells with this phenotype persisted for weeks and they exhibited enhanced effector function. Pathway analysis of genes enriched in NKT_{eff} in spleen following αGalCer alone, using the ConsensusPath Database, identified NK cell-mediated cytotoxicity as the most enriched pathway (Supplementary Fig. 4e). This is in line with the gene expression profile in these lymphocytes indicative of an enhanced effector phenotype found by GSEA (Fig. 5f). Intriguingly, there was similarity in chromatin accessibility in some key loci between NKT_{eff} and splenic NK cells, with increased ATAC-seq peaks within the loci for genes encoding Granzyme A and B, KLRG1 and CX3CR1, as well as Spry2, which is also highly expressed by NK cells (Fig. 6a). There also were some regions of increased chromatin accessibility in

bioRxiv preprint doi: https://doi.org/10.1101/2020.10.27.357673; this version posted October 27, 2020. The copyright holder for this preprint (which was not certified by peer review) is the author/funder. All rights reserved. No reuse allowed without permission.

genes associated with NK cell function in NKT1 cells, but these regions had higher signals in NKT_{eff} and NK cells.

To validate the existence of the NKT_{eff} population, we assessed the expression of KLRG1 and CX3CR1, NK cell markers with increased chromatin accessibility in NKT_{eff} (Fig. 6a). We detected increased expression of each of these markers on NKT_{eff} compared to NKT_{FH} and iNKT cells from uninjected mice (Fig. 6b). T-bet fate-mapping analysis revealed that virtually all $KLRG1^+$ NKT_{eff} had expressed T-bet, suggesting either these cells differentiated from NKT1 cells or acquired expression T-bet when activated (Fig. 5g). To determine if the phenotypic changes we observed were maintained, we also analyzed splenic iNKT cell populations at day 30 or later after antigen exposure. iNKT cells with the NKT_{eff} phenotype were still a sizeable fraction of the iNKT cells (Fig. 6c). Similarly, NKT_{FH} cells also persisted in the spleen beyond day 30 (Supplementary Fig. 4f), consistent with a report showing elevation of NKT_{FH} 60 days post-treatment with αGalCer and ovalbumin-loaded liposomes[32]. These data suggest that antigen challenge induces dynamic and prolonged changes in the phenotype of iNKT cells reflecting changes in the transcriptome and chromatin landscape.

bioRxiv preprint doi: https://doi.org/10.1101/2020.10.27.357673; this version posted October 27, 2020. The copyright holder for this preprint (which was not certified by peer review) is the author/funder. All rights reserved. No reuse allowed without permission.

Discussion

There are functional subsets of iNKT cells, analogous to CD4 T_{H1}, T_{H2} and T_{H17} cells, as well as several other lymphocyte populations[7], and it has been established that the chromatin landscape and transcriptomes of the thymic iNKT cell subsets are distinct[7, 12]. Here, we addressed three questions. First, to what extent are the gene programs driving the thymic iNKT cell subsets present in peripheral iNKT cells? Second, considering that iNKT cells are mostly non-recirculating lymphocytes[11], what is the imprint of localization in different tissues on these gene programs? Third, to what extent are the iNKT cell gene programs subject to dynamic and long-term changes following antigenic stimulation, as such changes might be suggestive of trained immunity or an effector-memory response?

Our data indicated that the status of chromatin accessibility and the transcriptome in any one subset are relatively similar to one another, regardless of location. Although this suggests that iNKT cells become fully mature and committed to a subset in the thymus and maintain their status in the periphery, there is evidence based on the expression of diagnostic surface proteins that iNKT cell recent thymic emigrants are not fully mature[33, 34, 35]. Perhaps the epigenome of the iNKT cell subsets is set up in the thymus prior to emigration, but with the mature, subset-specific transcriptome only initiated after thymus emigration. ATAC-seq analysis of stage 0, stage 1 and mature NKT1 cells identified regions accessible in mature NKT1 cells were already accessible in stage 0 cells, providing further evidence to support this hypothesis[36]. Alternatively, it is possible that the recent thymic emigrants are not fully differentiated but receive

bioRxiv preprint doi: https://doi.org/10.1101/2020.10.27.357673; this version posted October 27, 2020. The copyright holder for this preprint (which was not certified by peer review) is the author/funder. All rights reserved. No reuse allowed without permission.

tissue-specific cues allowing the cells to mature into an effector subset resembling their thymic counterparts.

Although the imprint of tissue localization was comparatively limited, in the lung iNKT cells exhibited motif enrichment in regions of accessible chromatin for bZIP domain transcription factors, which can include AP-1 and ATF, and RHD (NF-κB) transcription factors, regardless of the functional subset. This may be related to an activation signature, consistent with the increased CTLA-4 expression by lung iNKT cells. These data are consistent with a recent report describing a similar gene expression signature in lung MAIT and iNKT cells, although it was also consistent with a tissue-residency pattern[11]. Regardless, the lung signature was present not only in iNKT cell subsets, but also in NK cells and γδ T cells, and to a lesser extent even in $CD4^+$ T cells compared to the corresponding cell type in the spleen. A recent study comparing the epigenome of alveolar $CD8^+$ resident memory T cells (Trm) found that Trm cells within the lung interstitial space were enriched for AP-1, FOS and CREM motifs compared to splenic Trm[37]. In other studies, this lung signature was not just specific to lymphocytes, with some similarities to the lung epigenome of alveolar macrophages[38]. Based on these findings and the present study, the lung microenvironment may dictate epigenetic remodeling and subsequent transcriptional changes. One potentially important factor is increased oxygen concentration[39, 40], and also, the lung may face more environmental exposure to external substances and microbes[40]. Perhaps immune cells in the lung need to be poised to rapidly respond to challenges. If this were correct, then we would predict that iNKT cells in sites such as skin or intestine might also have gene programs

bioRxiv preprint doi: https://doi.org/10.1101/2020.10.27.357673; this version posted October 27, 2020. The copyright holder for this preprint (which was not certified by peer review) is the author/funder. All rights reserved. No reuse allowed without permission.

distinct from cells in thymus, spleen and liver. Consistent with this hypothesis, we found increased CTLA-4 expression on iNKT cells from the SI-LPL. Additionally, iNKT cells from the the draining lymph nodes of the lung and the small intestine, the inguinal lymph node and mesenteric lymph node, express a large number of lung signature genes including *Fos*, *Fosb*, and *Nr4a1* compared to the thymus and spleen[35]. A more detailed exploration of the lung activation signature in iNKT cells and other innate populations within antigen exposed tissues is needed.

Six days after antigenic exposure, we detected two different iNKT cell populations, one is NKT_{FH} that is similar to T_{FH}. Previously, NKT_{FH} were reported, based on expression of BCL-6, a few key surface proteins, and functional assays for T cell help[26]. Here, we demonstrated that this NKT_{FH} population has a dramatically different chromatin landscape and transcriptome that resembles T_{FH}. These cells likely originated in part from NKT1, the major splenic subset population, but probably also from other activated subsets considering reduced prior T-bet expression, and they persisted for at least 30 days after antigenic challenge. At later time points, NKT_{FH} maintain the capacity to produce IL-21, but downregulate BCL-6 expression and increase expression of CD62L and CCR7, consistent with memory T_{FH}[32]. As detected by immune assays, the half-life of αGalCer complexes with CD1d on the surface of DCs *in vivo* was less than 24h[41, 42]. Given this half-life, it is unlikely that these cells experience any recent exposure to αGalCer. Therefore, chromatin remodeling in iNKT cells after antigen exposure led to the generation of a persisting population of iNKT cells that is expected to have enhanced helper function for B cells.

bioRxiv preprint doi: https://doi.org/10.1101/2020.10.27.357673; this version posted October 27, 2020. The copyright holder for this preprint (which was not certified by peer review) is the author/funder. All rights reserved. No reuse allowed without permission.

411

412 The second population called NKT_{eff} more closely resembled NK cells. iNKT cells with
413 this phenotype also were present for at least 30 days. Previously a similar population
414 was present in lung after injection of antigen-loaded DCs[31], but here we show that
415 NKT_{eff} can be generated systemically following the same antigenic challenge that also
416 induces the NKT_{FH} population. In other experiments, it was reported that iNKT cells
417 exposed to αGalCer were anergic for many weeks[43, 44]. In previous work, we did not
418 find evidence for anergy in the total iNKT cell population, because at 30 days following
419 αGalCer, re-challenged iNKT cells remained cytotoxic, effectively signaled through their
420 TCR, and had increased proliferation compared to iNKT cells responding to αGalCer for
421 the first time[45]. However, we did find reduced pro-inflammatory cytokine production,
422 which could reflect the distinct functions of NKT_{FH} cells that were likely generated, and a
423 minority of the iNKT cells that acquired the ability to produce IL-10[45]. Therefore, it is
424 likely that iNKT cells from mice injected with antigen that did not become NKT_{FH} are
425 heterogenous, including not only NKT_{eff} but IL-10 producers and perhaps some anergic
426 cells. Further, in studies of $KLRG1^+$ iNKT cell induction by antigen-loaded DCs, these
427 cells maintain long-term anti-tumor function[31]. The size of the NKT_{eff} population is
428 difficult to quantify because $KLRG1^+$ cells accounted for only a portion, with other cells
429 expressing high amounts of CX3CR1 and granzymes (Fig. 6b, d). The contributions of
430 TCR signal strength, co-stimulation, cytokines and other aspects to the generation of
431 disparate iNKT cell populations remain to be determined, but apparently pulsing DC
432 with αGalCer is a more effective method for generating NKT_{eff} almost exclusively in the
433 lung[31].

bioRxiv preprint doi: https://doi.org/10.1101/2020.10.27.357673; this version posted October 27, 2020. The copyright holder for this preprint (which was not certified by peer review) is the author/funder. All rights reserved. No reuse allowed without permission.

iNKT cells have been classified as innate-like T lymphocytes that bridge the innate and adaptive immune systems, sharing components of cells within each major branch of the immune response[5]. The capacity for innate-like cells to exhibit long-term changes in their functional programs in response to antigen exposure has been referred to as trained immunity[46]. Do iNKT cells exhibit an effector memory response or a form of trained immunity? At steady-state, iNKT cells have some properties of tissue-resident memory cells. Many of them express molecules characteristic of canonical resident memory T cells, such as CD103 and CD69, and like effector memory cells, they produce cytokines in a TCR-dependent or cytokine-dependent manner within a few hours[9, 11]. In response to αGalCer, however, dynamic, long-term changes occur in iNKT cells, generating NKT_{FH}, NKT_{eff} populations, and likely others, indicating a degree of plasticity and heterogeneity that allow these cells to adapt to their history of prior antigenic stimulation and respond in a variety of contexts.

Materials and Methods

Mice

C57BL/6J female mice aged 6-8 weeks old were purchased from Jackson Laboratories or bred in-house at La Jolla Institute for Immunology. B6;CBA-Tg(Tbx21-cre)1Dlc/J (Tbet-cre) were purchased from Jackson Laboratories and then bred with B6.Cg-Gt(ROSA)26Sor$^{tm14(CAG-tdTomato)Hze/J}$ (Td-tomato) mice (also obtained from Jackson Laboratories) to generate the T-bet fate mapping line. All studies were

bioRxiv preprint doi: https://doi.org/10.1101/2020.10.27.357673; this version posted October 27, 2020. The copyright holder for this preprint (which was not certified by peer review) is the author/funder. All rights reserved. No reuse allowed without permission.

457 approved by the Institutional Animal Care and Use Committee at the La Jolla Institute
458 for Immunology.
459
460 *Tissue Preparation*
461 Following euthanasia, thymus tissue and spleens were removed, lungs and livers were
462 perfused with 3-10 mL of liver perfusion medium (Gibco) until tissues cleared. Livers
463 were mashed through a 70 μM nylon filter (Fisher). Liver lymphocytes were isolated by
464 centrifugation at 850x*g* in 37.5% Percoll for 20 minutes. Lungs were placed in
465 GentleMacs C tubes (Miltenyi Biotec) with 2 mL Spleen Dissociation Medium
466 (STEMCELL Technologies) and homogenized using the Miltenyi GentleMacs
467 dissociator. Following homogenization, suspensions were filtered with a 70 μM filter
468 and washed twice with RPMI + 10% FBS. Thymus and spleens were homogenized
469 through a 70 μM nylon filter and washed with RPMI + 10% FBS. For lamina propria
470 lymphocyte isolation, small intestines were collected from mice and Peyer's patches
471 removed. The tissue was washed and cut into pieces that were then incubated in 25 ml
472 of HBSS (5% FBS, 25mM HEPES and 1mM DTT) in a shaker at 225 r.p.m., 37°C, for
473 20 min. Samples were filtered and the tissue debris was incubated in 20 ml of HBSS
474 (25mM HEPES and 20mM EDTA) in a shaker at 225 r.p.m., 37°C, 2 times for 15 min to
475 further remove epithelial cells. Then, tissues were incubated at 37°C for 25 min with
476 rotation in media containing collagenase type VIII (Sigma). The filtered cell suspension
477 was re-suspended in 40% Percoll solution and overlaid above 80% Percoll solution. LPL
478 were collected from the interface.
479

bioRxiv preprint doi: https://doi.org/10.1101/2020.10.27.357673; this version posted October 27, 2020. The copyright holder for this preprint (which was not certified by peer review) is the author/funder. All rights reserved. No reuse allowed without permission.

Antigen challenge

α-galactosyl ceramide (αGalCer or KRN7000) was supplied as a lyophilizate in vehicle and provided by Kyowa Kirin Pharmaceutical Research. It was resuspended at 200 µg/mL in water and then diluted to 10 µg/mL in PBS. 0.2 mL of 10 µg/mL αGalCer was administered via retro-orbital injection, and 6- or ≥30-days later mice were euthanized and organs harvested.

Cell Sorting

For RNA-seq and ATAC-seq experiments, unless otherwise noted iNKT cell subsets were sorted in parallel from tissues pooled from 15-20 female C57BL/6J mice, approximately 6 weeks of age. Cell suspensions from thymus, spleen and lung were enriched for iNKT cells by negative selection using biotinylated antibodies against CD8α (53–6.7, BD Biosciences), CD19 (1D3, Tonbo Biosciences), CD24 (M1/69, BD Biosciences), CD62L (MEL-14, Invitrogen), CD11b (M1/70, Tonbo Biosciences), CD11c (N418, Tonbo Biosciences), F4/80 (BM5.1, Tonbo Biosciences), EpCam(G8.8, BioLegend), and TER-119 (TER-119, Tonbo Biosciences) together with Rapidspheres (StemCell technologies) and either the Big Easy or Easy eight magnets (StemCell technologies) using protocols from the manufacturer. The remaining cells were then suspended at 10^8 cells/mL, incubated with 1 µg/mL of Streptavidin A (Sigma-Aldrich). Liver lymphocytes were not enriched for iNKT cells. iNKT cells were stained using a 12-parameter panel of reagents including tetramers of CD1d loaded with αGalCer (BV421, in house preparation), live/dead yellow (ThermoFisher Scientific), anti-TCRβ-APC-eF780 (H57-597, ThermoFisher Scientific), anti-CD8α-PE CF594 (53-6.7, BD

bioRxiv preprint doi: https://doi.org/10.1101/2020.10.27.357673; this version posted October 27, 2020. The copyright holder for this preprint (which was not certified by peer review) is the author/funder. All rights reserved. No reuse allowed without permission.

Biosciences) and anti-CD19-PE CF594 (1D3, BD Biosciences), anti-CD4-AF700 (GK1.5, BioLegend), anti-IL-17RB-AF488 (FAB10402G, R&D Systems), anti-ICOS-PerCP Cy5.5 (C398.4A, BioLegend), anti-CD122-BV650 (5H4, BD Biosciences), anti-CXCR3-APC (CXCR3-173, BioLegend), anti-SDC1-PE (281-2, BioLegend), and anti-FR4-PE Cy7 (ebio12A5, ThermoFisher Scientific). Cells were sorted using a FACSAria III or FACSAria Fusion (BD Biosciences) for live lymphocytes, singlets, $CD8^{-}CD19^{-}$, $Tetramer^{+}TCR\beta^{+}$ iNKT cells and separated into NKT1, NKT2, and NKT17 cell subsets based on the following expression profiles: NKT1: $CXCR3^{+}ICOS^{-}CD122^{+}SDC1^{-}IL\text{-}17RB^{-}$; NKT2: $CXCR3^{-}ICOS^{+}CD122^{-}SDC1^{-}IL\text{-}17RB^{+}CD4^{+}$; NKT17: $CXCR3^{-}ICOS^{+}CD122^{-}SDC1^{+}IL\text{-}17RB^{+}FR4^{-}$.

For NKT_{FH} sorts, spleens were harvested 6 days following antigen challenge. Single cell suspensions were enriched for iNKT cells as described above. iNKT cells were stained with CD1d tetramers loaded with αGalCer, live/dead yellow, anti-CD8α-PE CF594 and anti-CD19-PE CF594, anti-TCRβ-APC-eF780. NKT_{FH} cells were identified based on expression of CXCR5 (anti-CXCR5-PE, clone L138D7, BioLegend), and PD-1 (anti-PD-1-APC, clone RMP1-30, BioLegend). $CXCR5^{-}PD\text{-}1^{-}$ iNKT cells from antigen challenged mice were also sorted for comparison (NKT_{eff}).

For sorting of γδ T cells, $CD4^{+}$ T cells, NK cells, and iNKT cells from lung and spleen, tissues were prepared and enriched as described above. Populations were sorted based on the following gating strategy: live lymphocytes, singlets, $CD8^{-}CD19^{-}$; iNKT cells, $Tetramer^{+}TCR\beta^{+}$; γδ T cells, $TCR\beta^{-}TCR\gamma\delta^{+}$ (anti-TCRγδ-FITC , clone GL3, BD

bioRxiv preprint doi: https://doi.org/10.1101/2020.10.27.357673; this version posted October 27, 2020. The copyright holder for this preprint (which was not certified by peer review) is the author/funder. All rights reserved. No reuse allowed without permission.

Biosciences); NK cells, TCRβ$^-$, NK1.1$^+$ (anti-NK1.1-PE Cy7, clone PK136, BD Biosciences); CD4$^+$ T cells, TCRβ$^+$CD4$^+$.

Flow Cytometry

Cells isolated from the lung or spleen were stained for iNKT cell subsets, NKT_{FH} and NKT_{eff}, as described above. In addition to the antibodies and other reagents used for iNKT isolation described above, we also used anti-PLZF-AF647 (clone R17–809), anti-T-bet-AF488 (clone O4–46), anti-RORγt-PE-CF594 (clone Q31-378), anti-BCL-6-AF488 (clone K112-91), all from BD Biosciences, anti-KLRG1- PECy7 (clone 2F1), and anti-CTLA-4-PE (clone UC10-4B9), all from Thermo-Fisher Scientific, and anti-CX3CR1-BV711 (clone SA011F11, BioLegend). Staining for total CTLA-4 expression was performed according to a using Cytofix (BD Biosciences) and eBioscience permeabilization buffer (Thermo-Fisher Scientific). Stained samples were analyzed using a Fortessa flow cytometer (BD Biosciences) and FlowJo software (Treestar).

RNA-seq

Cells representing specific iNKT subsets were sorted by pools of cells ranging between 200 to 400 directly into 0.2 ml PCR tubes containing 8 µl of low-input lysis buffer (0.2% Triton-X-100 and RNase inhibitor) and stored at -80^{o}C until processed further. For thymic subsets, n = 5 (NKT1), n = 4 (NKT2), n = 6 (NKT17). For peripheral subsets, NKT1: lung n = 5, liver n = 5, spleen n = 7; NKT2: lung n = 6, spleen n = 7; NKT17: lung n = 7, spleen n = 6. For NKT_{FH}, n = 6, NKT_{eff}, n = 3. For lung cell types, NK: lung n = 3, spleen n = 4; γδ T cells: lung n = 3, spleen n = 3; CD4$^+$ T cells: lung n = 3, spleen n = 5.

bioRxiv preprint doi: https://doi.org/10.1101/2020.10.27.357673; this version posted October 27, 2020. The copyright holder for this preprint (which was not certified by peer review) is the author/funder. All rights reserved. No reuse allowed without permission.

549 For bulk library preparation for sequencing we used the Smart-Seq2 protocol[47], adapted
550 for samples with small cell numbers. We followed the protocol as described previously[19,
551 47] with following modifications: (i) the pre-amplification PCR cycle was set between 17
552 to 23 cycles; (ii) to eliminate any traces of primer-dimers, the PCR pre-amplified cDNA
553 product was purified using 0.8x Ampure-XP beads (Beckman Coulter) before using the
554 DNA for sequencing library preparation. One ng of pre-amplified cDNA was used to
555 generate barcoded Illumina sequencing libraries (Nextera XT library preparation kit -
556 Illumina) in 8 µl reaction volume. Samples failing any quality control step (DNA quality
557 assessed by capillary electrophoresis (Fragment analyzer, Advance analytical) and
558 quantity (Picogreen quantification assay, Thermofisher) were eliminated from further
559 downstream steps[19]. Libraries were then pooled at equal molar concentration and
560 quantified (KAPA SYBR® FAST qPCR Kit - Roche)[19]. Samples from the experiment
561 comparing splenic NKT_{FH} and NKT_{eff} cells from αGalCer-challenged mice with
562 unchallenged splenic iNKT cells were sequenced via a 100 x 100 bp paired-end read
563 strategy using the NovaSeq6000 sequencing platform (NovaSeq 6000 S4 P200 kits -
564 Illumina). Sequencing for all other samples was performed according to a 50 bp single-
565 end strategy using the HiSeq2500 sequencer (HiSeq SBS Kit v4; Illumina). Post-
566 sequencing, stringent quality controls were applied and samples that failed quality
567 control standards were eliminated from further analysis[19]. Samples we sequenced to
568 obtain at least 8 million uniquely mapped reads.
569
570 The single-end reads that passed Illumina filters were filtered for reads aligning to tRNA,
571 rRNA, adapter sequences, and spike-in controls. The reads were then aligned to mm10

bioRxiv preprint doi: https://doi.org/10.1101/2020.10.27.357673; this version posted October 27, 2020. The copyright holder for this preprint (which was not certified by peer review) is the author/funder. All rights reserved. No reuse allowed without permission.

reference genome using TopHat (v 1.4.1)[48]. DUST scores were calculated with PRINSEQ Lite (v 0.20.3)[49] and low-complexity reads (DUST > 4) were removed from the BAM files. The alignment results were parsed via the SAMtools[50] to generate SAM files. Read counts to each gene were obtained with the htseq-count program (v 0.7.1)[51] using the "union" option. After removing absent features (zero counts in all samples), the raw counts were then imported in most cases to the R/Bioconductor package DESeq2 (v 1.6.3)[52] to identify differentially expressed genes among samples, with P-values for differential expression calculated using the Wald test for differences between the base means of two conditions. For the analysis of iNKT samples collected after in vivo stimulation, the R/Bioconductor package EdgeR was used, and P values were determined using the quasi-likelihood F test. For determination of signature genes of specific iNKT subsets, we included genes that exhibited a 2-fold or greater expression difference with a P value of ≤0.1 in all pairwise comparisons between the given subset and the other two subsets in each of the organs from which all three subsets were collected (thymus, spleen and lung). Similarly, the signature genes of spleen, lung and thymus were defined as those genes exhibiting a fold change of ≥2 with a P value of ≤0.1 in all possible comparisons between the same iNKT subset from different organs. Signature genes of splenic iNKT populations that either expressed or lacked the FH markers PD-1 and CXCR5 after αGalCer stimulation were determined in a similar fashion, except that P-values were adjusted for multiple test correction using Benjamini Hochberg algorithm[50], and both stimulated populations were also compared to unchallenged total splenic iNKT. Principal Component Analysis (PCA) was performed using the 'prcomp' function in R. The sequences used in this article will be submitted to

bioRxiv preprint doi: https://doi.org/10.1101/2020.10.27.357673; this version posted October 27, 2020. The copyright holder for this preprint (which was not certified by peer review) is the author/funder. All rights reserved. No reuse allowed without permission.

595 the Gene Expression Omnibus and the accession number will be reported prior to
596 publication (http://www.ncbi.nlm.nih.gov/geo/). Data were also analyzed using the Pre-
597 ranked Gene Set Enrichment Analysis algorithm (Broad Institute and University of
598 California), as well as the Consensus Path Database platform (Max Planck Institute).
599
600 *ATAC-seq*
601 ATAC-seq was performed as previously described with some modifications[13]. For
602 thymic subsets, n = 4 (NKT1), n = 4 (NKT2), n = 3 (NKT17). For peripheral subsets,
603 NKT1: lung n = 3, liver n = 2, spleen n = 2; NKT2: lung n = 1, spleen n = 2; NKT17: lung
604 n = 2, spleen n = 2. For NKT_{FH}, n = 6, NKT_{eff}, n = 3. For lung cell types, NK: lung n = 1,
605 spleen n = 2; γδ T cells: lung n = 2, spleen n = 3; $CD4^+$ T cells: lung n = 2, spleen n = 3.
606 iNKT cells or lung lymphocytes (10,000) were sorted into 1.5 mL Eppendorf tubes
607 containing PBS with 5% FCS. Cells were centrifuged at 600*g* for 10 minutes at 4°C,
608 washed with 50 μL PBS, then resuspended in 50 μL ATAC lysis buffer (10 mM Tris pH
609 7.5, 10 mM NaCl, 3 mM $MgCl_2$, 0.1% NP-40). Cells were centrifuged in lysis buffer for
610 10 minutes at 600*g*, 4°C. Following lysis, the pellet was resuspended in 50 μL ATAC
611 reaction mix (25uL 2X TD buffer, 2.5 μL Nextera Enzyme, 22.5 μL water, Illumina). The
612 transposase reaction was carried out at 37°C for 30 minutes. Libraries were amplified
613 using a KAPA HiFi real-time library amplification kit with barcoded primers for 11-12
614 cycles followed by 2x50 cycle paired-end sequencing. Reads were mapped to mouse
615 genome (mm9) using bowtie. Unmapped reads were processed with trim galore, re-
616 mapped with bowtie and merged with previous mapping output. Duplicate reads
617 identified by picard MarkDuplicates and reads mapping to chrM were excluded. Wiggle

bioRxiv preprint doi: https://doi.org/10.1101/2020.10.27.357673; this version posted October 27, 2020. The copyright holder for this preprint (which was not certified by peer review) is the author/funder. All rights reserved. No reuse allowed without permission.

files of coverage for individual replicates were computed with MEDIPS[51] using full fragments captured by ATAC-seq on 10 bp windows and used to generate average coverage with the Java Genomics Toolkit (available at: https://github.com/timpalpant/java-genomics-toolkit) for each group. Accessible regions were identified using MACS2[52] from individual replicate bam files downsampled to a maximum of 5 million reads and limited to a q value of less than 0.001. Peaks that intersected ENCODE blacklisted regions and those on chromosome Y were excluded. We refined the groups of accessible regions to non-overlapping peaks with a uniform width of 500 nucleotides with the readNarrowpeaks function from chromVAR[53]. The number of reads within each region was computed using all reads from each replicate with the getCounts function from chromVAR. Differentially accessible regions were identified with limma/voom, using quantile normalized counts, and selected based on an fdr adjusted p value of less than 0.1 and an estimated fold change of at least 4. We associated transcription factors binding motifs from the HOMER database by determining the enrichment of motifs in groups of peaks with HOMER and comparing the variability in ATAC-seq signal with chromVAR.

Acknowledgements

We thank Shu Liang, Alice Wang, Monalisa Mondal and Jeremy Day for assistance with next generation sequencing and the Flow Cytometry Core Facility at the La Jolla Institute for Immunology for assistance with cell sorting. We thank Archana Khurana for generating CD1d-αGalCer tetramers. We thank Anjana Rao for critical feedback on the manuscript. Supported by the US National Institutes of Health R01 AI71922, AI105215,

bioRxiv preprint doi: https://doi.org/10.1101/2020.10.27.357673; this version posted October 27, 2020. The copyright holder for this preprint (which was not certified by peer review) is the author/funder. All rights reserved. No reuse allowed without permission.

AI137230 to M.K.; R01 AI040127 and AI109842 to Anjana Rao and Patrick Hogan; T32 AI125179 to M.P.M.; Shared Instrumentation Grant (SIG) Program S10 OD018499 to the Flow Cytometry Core Facility at the La Jolla Institute for Immunology; S10 RR027366 for a FACSAria II cell sorter to Dr. Michael Croft; S10 OD016262 for an Illumina HiSeq 2500 sequencing system to Dr. Anjana Rao; S10 OD025052 for a NovaSeq 6000 sequencer to Dr. Gregory Seumois.

Author Contributions

M.P.M., I.E. and G.S. designed and performed experiments and analyzed data. S.H.M., S.L.R. and G-Y.S. performed experiments. A.S., A.L.R.P. and J.G. analyzed the RNA-seq data. P.V. designed the study. J.S.B. analyzed the ATAC-seq data. M.P.M and M.K. wrote the manuscript. J.S.B and M.K. supervised the project, designed the study, and analyzed data.

Competing interests

The authors declare no competing interests.

References

1. Mori, L., Lepore, M. & De Libero, G. The Immunology of CD1- and MR1-Restricted T Cells. *Annu Rev Immunol* **34**, 479-510 (2016).

2. Godfrey, D.I. & Kronenberg, M. Going both ways: Immune regulation via CD1d-dependent NKT cells. *Journal of Clinical Investigation* **114**, 1379-1388 (2004).

3. Verykokakis, M., Zook, E.C. & Kee, B.L. ID'ing innate and innate-like lymphoid cells. *Immunol Rev* **261**, 177-197 (2014).

bioRxiv preprint doi: https://doi.org/10.1101/2020.10.27.357673; this version posted October 27, 2020. The copyright holder for this preprint (which was not certified by peer review) is the author/funder. All rights reserved. No reuse allowed without permission.

4. Godfrey, D.I., Koay, H.F., McCluskey, J. & Gherardin, N.A. The biology and functional importance of MAIT cells. *Nat Immunol* **20**, 1110-1128 (2019).

5. Godfrey, D.I., Uldrich, A.P., McCluskey, J., Rossjohn, J. & Moody, D.B. The burgeoning family of unconventional T cells. *Nat Immunol* **16**, 1114-1123 (2015).

6. Lee, Y. *et al.* Tissue-Specific Distribution of iNKT Cells Impacts Their Cytokine Response. *Immunity* **43**, 566-578 (2015).

7. Lee, Y. *et al.* Lineage-Specific Effector Signatures of Invariant NKT Cells Are Shared amongst γδ T, Innate Lymphoid, and Th Cells. *The Journal of Immunology* **197**, 1460-1470 (2016).

8. Engel, I. *et al.* Innate-like functions of natural killer T cell subsets result from highly divergent gene programs. *Nature Immunology* **17**, 728-739 (2016).

9. Crosby, C.M. & Kronenberg, M. Tissue-specific functions of invariant natural killer T cells. *Nat Rev Immunol* **18**, 559-574 (2018).

10. Lynch, L. *et al.* Regulatory iNKT cells lack expression of the transcription factor PLZF and control the homeostasis of Treg cells and macrophages in adipose tissue. *Nature Immunology* **16**, 85-95 (2015).

11. Salou, M. *et al.* A common transcriptomic program acquired in the thymus defines tissue residency of MAIT and NKT subsets. *J Exp Med* **216**, 133-151 (2019).

12. Georgiev, H., Ravens, I., Benarafa, C., Forster, R. & Bernhardt, G. Distinct gene expression patterns correlate with developmental and functional traits of iNKT subsets. *Nat Commun* **7**, 13116 (2016).

13. Buenrostro, J.D., Giresi, P.G., Zaba, L.C., Chang, H.Y. & Greenleaf, W.J. Transposition of native chromatin for fast and sensitive epigenomic profiling of open chromatin, DNA-binding proteins and nucleosome position. *Nature Methods* **10**, 1213-1218 (2013).

14. Scott-Browne, J.P. *et al.* Dynamic Changes in Chromatin Accessibility Occur in CD8+ T Cells Responding to Viral Infection. *Immunity* **45**, 1327-1340 (2016).

15. Scharer, C.D., Bally, A.P., Gandham, B. & Boss, J.M. Cutting Edge: Chromatin Accessibility Programs CD8 T Cell Memory. *J Immunol* **198**, 2238-2243 (2017).

16. Lee, D.U., Avni, O., Chen, L. & Rao, A. A Distal Enhancer in the Interferon-γ (IFN-γ) Locus Revealed by Genome Sequence Comparison. *Journal of Biological Chemistry* **279**, 4802-4810 (2004).

bioRxiv preprint doi: https://doi.org/10.1101/2020.10.27.357673; this version posted October 27, 2020. The copyright holder for this preprint (which was not certified by peer review) is the author/funder. All rights reserved. No reuse allowed without permission.

17. Berga-Bolanos, R., Zhu, W.S., Steinke, F.C., Xue, H.H. & Sen, J.M. Cell-autonomous requirement for TCF1 and LEF1 in the development of Natural Killer T cells. *Mol Immunol* **68**, 484-489 (2015).

18. Carr, T. *et al.* The transcription factor lymphoid enhancer factor 1 controls invariant natural killer T cell expansion and Th2-type effector differentiation. *J Exp Med* **212**, 793-807 (2015).

19. Rosales, S.L. *et al.* A Sensitive and Integrated Approach to Profile Messenger RNA from Samples with Low Cell Numbers. *Methods Mol Biol* **1799**, 275-302 (2018).

20. Lazarevic, V. *et al.* The gene encoding early growth response 2, a target of the transcription factor NFAT, is required for the development and maturation of natural killer T cells. *Nat Immunol* **10**, 306-313 (2009).

21. Aliahmad, P. & Kaye, J. Development of all CD4 T lineages requires nuclear factor TOX. *J Exp Med* **205**, 245-256 (2008).

22. Chen, Y.G. *et al.* CD38 is required for the peripheral survival of immunotolerogenic CD4+ invariant NK T cells in nonobese diabetic mice. *J Immunol* **177**, 2939-2947 (2006).

23. Huynh, H., Ng, C.Y., Ong, C.K., Lim, K.B. & Chan, T.W. Cloning and characterization of a novel pregnancy-induced growth inhibitor in mammary gland. *Endocrinology* **142**, 3607-3615 (2001).

24. Tsagaratou, A. *et al.* TET proteins regulate the lineage specification and TCR-mediated expansion of iNKT cells. *Nat Immunol* **18**, 45-53 (2017).

25. Best, J.A. *et al.* Transcriptional insights into the CD8(+) T cell response to infection and memory T cell formation. *Nat Immunol* **14**, 404-412 (2013).

26. Chang, P.-P. *et al.* Identification of Bcl-6-dependent follicular helper NKT cells that provide cognate help for B cell responses. *Nature Immunology* **13**, 35-43 (2011).

27. Gaya, M. *et al.* Initiation of Antiviral B Cell Immunity Relies on Innate Signals from Spatially Positioned NKT Cells. *Cell* **172**, 517-1082130432 (2018).

28. Choi, Y.S. *et al.* LEF-1 and TCF-1 orchestrate T(FH) differentiation by regulating differentiation circuits upstream of the transcriptional repressor Bcl6. *Nat Immunol* **16**, 980-990 (2015).

29. Yu, F., Sharma, S., Edwards, J., Feigenbaum, L. & Zhu, J. Dynamic expression of transcription factors T-bet and GATA-3 by regulatory T cells maintains immunotolerance. *Nat Immunol* **16**, 197-206 (2015).

bioRxiv preprint doi: https://doi.org/10.1101/2020.10.27.357673; this version posted October 27, 2020. The copyright holder for this preprint (which was not certified by peer review) is the author/funder. All rights reserved. No reuse allowed without permission.

30. Shimizu, K. *et al.* Eomes transcription factor is required for the development and differentiation of invariant NKT cells. *Commun Biol* **2**, 150 (2019).

31. Shimizu, K. *et al.* KLRG+ invariant natural killer T cells are long-lived effectors. *Proc Natl Acad Sci U S A* **111**, 12474-12479 (2014).

32. Chen, Z. *et al.* Memory Follicular Helper Invariant NKT Cells Recognize Lipid Antigens on Memory B Cells and Elicit Antibody Recall Responses. *J Immunol* **200**, 3117-3127 (2018).

33. Wang, H. & Hogquist, K.A. CCR7 defines a precursor for murine iNKT cells in thymus and periphery. *Elife* **7** (2018).

34. Pellicci, D.G. *et al.* A Natural Killer T (NKT) Cell Developmental Pathway Involving a Thymus-dependent NK1.1−CD4+ CD1d-dependent Precursor Stage. *The Journal of Experimental Medicine* **195**, 835-844 (2002).

35. Jimeno, R. *et al.* Tissue-specific shaping of the TCR repertoire and antigen specificity of iNKT cells. *Elife* **8** (2019).

36. Gioulbasani, M. *et al.* The transcription factor BCL-6 controls early development of innate-like T cells. *Nat Immunol* **21**, 1058-1069 (2020).

37. Hayward, S.L. *et al.* Environmental cues regulate epigenetic reprogramming of airway-resident memory CD8(+) T cells. *Nat Immunol* **21**, 309-320 (2020).

38. Lavin, Y. *et al.* Tissue-resident macrophage enhancer landscapes are shaped by the local microenvironment. *Cell* **159**, 1312-1326 (2014).

39. Carreau, A., El Hafny-Rahbi, B., Matejuk, A., Grillon, C. & Kieda, C. Why is the partial oxygen pressure of human tissues a crucial parameter? Small molecules and hypoxia. *J Cell Mol Med* **15**, 1239-1253 (2011).

40. O'Dwyer, D.N., Dickson, R.P. & Moore, B.B. The Lung Microbiome, Immunity, and the Pathogenesis of Chronic Lung Disease. *J Immunol* **196**, 4839-4847 (2016).

41. Halder, R.C. *et al.* Self-glycerophospholipids activate murine phospholipid-reactive T cells and inhibit iNKT cell activation by competing with ligands for CD1d loading. *Eur J Immunol* **49**, 242-254 (2019).

42. Sullivan, B.A. *et al.* Mechanisms for glycolipid antigen-driven cytokine polarization by Valpha14i NKT cells. *J Immunol* **184**, 141-153 (2010).

43. Parekh, V.V. *et al.* Glycolipid antigen induces long-term natural killer T cell anergy in mice. *J Clin Invest* **115**, 2572-2583 (2005).

bioRxiv preprint doi: https://doi.org/10.1101/2020.10.27.357673; this version posted October 27, 2020. The copyright holder for this preprint (which was not certified by peer review) is the author/funder. All rights reserved. No reuse allowed without permission.

44. Fujii, S., Shimizu, K., Kronenberg, M. & Steinman, R.M. Prolonged IFN-gamma-producing NKT response induced with alpha-galactosylceramide-loaded DCs. *Nat Immunol* **3**, 867-874 (2002).

45. Sag, D., Krause, P., Hedrick, C.C., Kronenberg, M. & Wingender, G. IL-10–producing NKT10 cells are a distinct regulatory invariant NKT cell subset. *Journal of Clinical Investigation* **124**, 3725-3740 (2014).

46. Netea, M.G. *et al.* Trained immunity: A program of innate immune memory in health and disease. *Science* **352**, aaf1098 (2016).

47. Picelli, S. *et al.* Smart-seq2 for sensitive full-length transcriptome profiling in single cells. *Nat Methods* **10**, 1096-1098 (2013).

48. Trapnell, C., Pachter, L. & Salzberg, S.L. TopHat: discovering splice junctions with RNA-Seq. *Bioinformatics* **25**, 1105-1111 (2009).

49. Schmieder, R. & Edwards, R. Quality control and preprocessing of metagenomic datasets. *Bioinformatics* **27**, 863-864 (2011).

50. Li, H. *et al.* The Sequence Alignment/Map format and SAMtools. *Bioinformatics* **25**, 2078-2079 (2009).

51. Anders, S., Pyl, P.T. & Huber, W. HTSeq--a Python framework to work with high-throughput sequencing data. *Bioinformatics* **31**, 166-169 (2015).

52. Love, M.I., Huber, W. & Anders, S. Moderated estimation of fold change and dispersion for RNA-seq data with DESeq2. *Genome Biol* **15**, 550 (2014).

Data Availability Statement

Sequence data that support the findings of this study will be deposited in the Gene Expression Omnibus and the accession codes will be provided prior to publication.

ATAC-seq sequence data associated figures: Figure 1; Figure 2a, b, c; Figure 3 a, c; Figure 4a; Figure 5 a, b, c; Figure 6b.

bioRxiv preprint doi: https://doi.org/10.1101/2020.10.27.357673; this version posted October 27, 2020. The copyright holder for this preprint (which was not certified by peer review) is the author/funder. All rights reserved. No reuse allowed without permission.

RNA-seq sequence data associated figures: Figure 2d; Figure 3b; Figure 4 b, c, d, e; Figure 5 d, e, f; Figure 6a; Supplementary Figure 2; Supplementary Figure 3; Supplementary Figure 4 c, d.

There are no restrictions on data availability. Additional information and materials will be made available upon request.

Figures

bioRxiv preprint doi: https://doi.org/10.1101/2020.10.27.357673; this version posted October 27, 2020. The copyright holder for this preprint (which was not certified by peer review) is the author/funder. All rights reserved. No reuse allowed without permission.

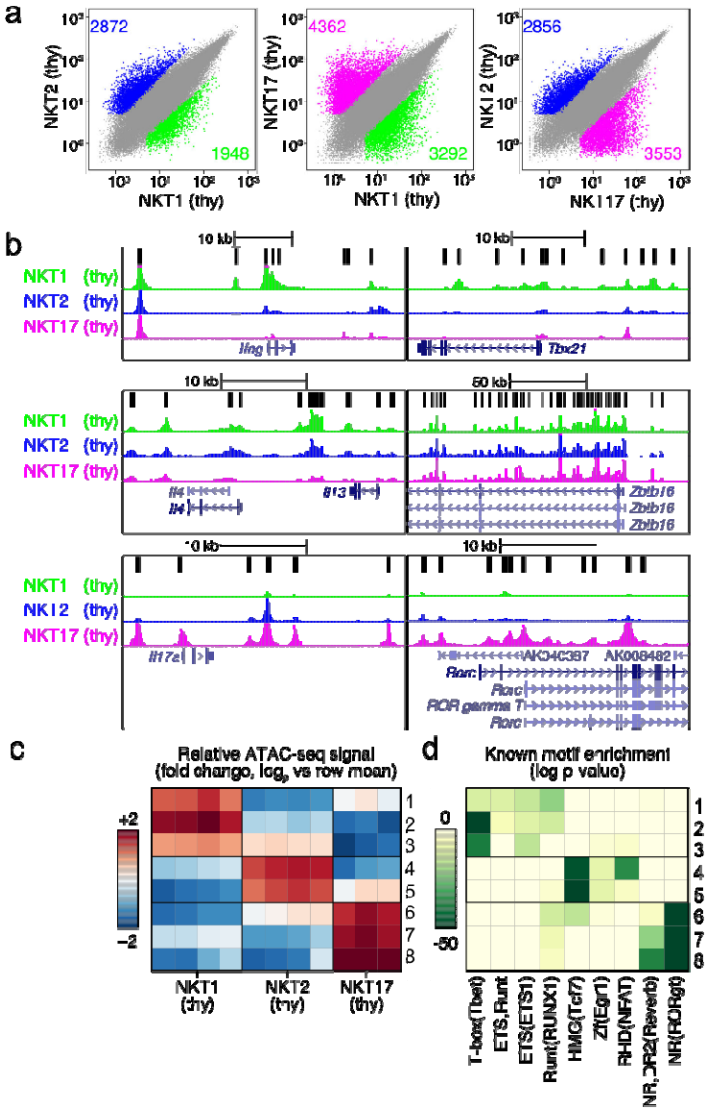

Fig. 1. Subsets of thymic iNKT cells have differences in chromatin accessibility. a. Scatterplot of mean ATAC-seq counts per peak comparing differentially accessible regions of chromatin for pairs of thymic iNKT cell subsets. Colors indicate differentially accessible regions defined by limma/voom (details in Methods). The numbers of differentially expressed genes are indicated. b. ATAC-seq coverage at the indicated gene loci with a range of 0-600 for all samples. Grey bar in the upper left panel (*Ifng*) locus indicates enhancer region. c. Left, *k*-means clustering of relative ATAC-seq density (counts per million mapped reads/kb, $\log_2$ fold change from the mean) identifies eight groups of accessible regions that varied similarly (rows), 3 sets for NKT1, 2 for NKT2 and 3 for NKT17. Columns indicate number of replicates, 3 or 4. d. Motifs enriched in enriched in clusters of accessible regions. All motifs with a HOMER log p-value less than –15 and found in 10% or more regions in at least one cluster are shown.

bioRxiv preprint doi: https://doi.org/10.1101/2020.10.27.357673; this version posted October 27, 2020. The copyright holder for this preprint (which was not certified by peer review) is the author/funder. All rights reserved. No reuse allowed without permission.

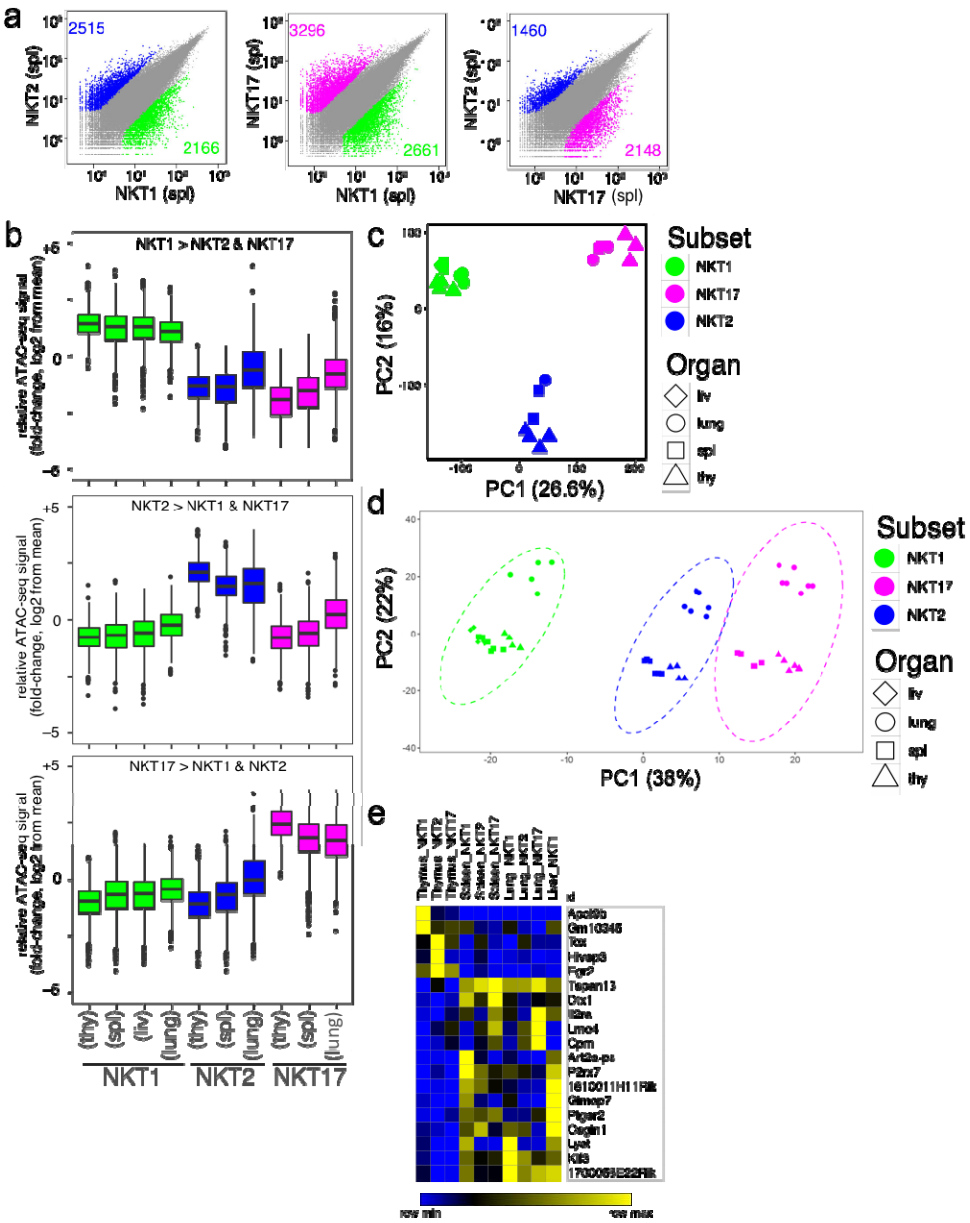

873

874 **Fig. 2. Imprint of tissue location is minor compared to subset.** a. Scatterplot of
875 mean ATAC-seq counts per peak comparing differentially accessible regions of
876 chromatin for pairs of iNKT cell subsets in spleen. Colors indicate differentially
877 accessible regions defined by limma/voom (details in Methods). b. Boxplot of
878 normalized average ATAC-seq counts per peak from the indicated samples (labeled at
879 bottom) at differentially-accessible regions that distinguish thymic iNKT cell subsets.
880 Box indicates interquartile range with whiskers +/−1.5 times this range and outlier points
881 indicated. c, d. PCA display of ATACseq (c) and RNA-seq (d) data from the indicated
882 iNKT cell subsets from the different tissues. e. Heat map of normalized reads from
883 RNA-seq for genes (19) differentially regulated in thymus versus peripheral iNKT cell
884 subsets, within all subsets, n > 2-fold difference, p = 0.1.

bioRxiv preprint doi: https://doi.org/10.1101/2020.10.27.357673; this version posted October 27, 2020. The copyright holder for this preprint (which was not certified by peer review) is the author/funder. All rights reserved. No reuse allowed without permission.

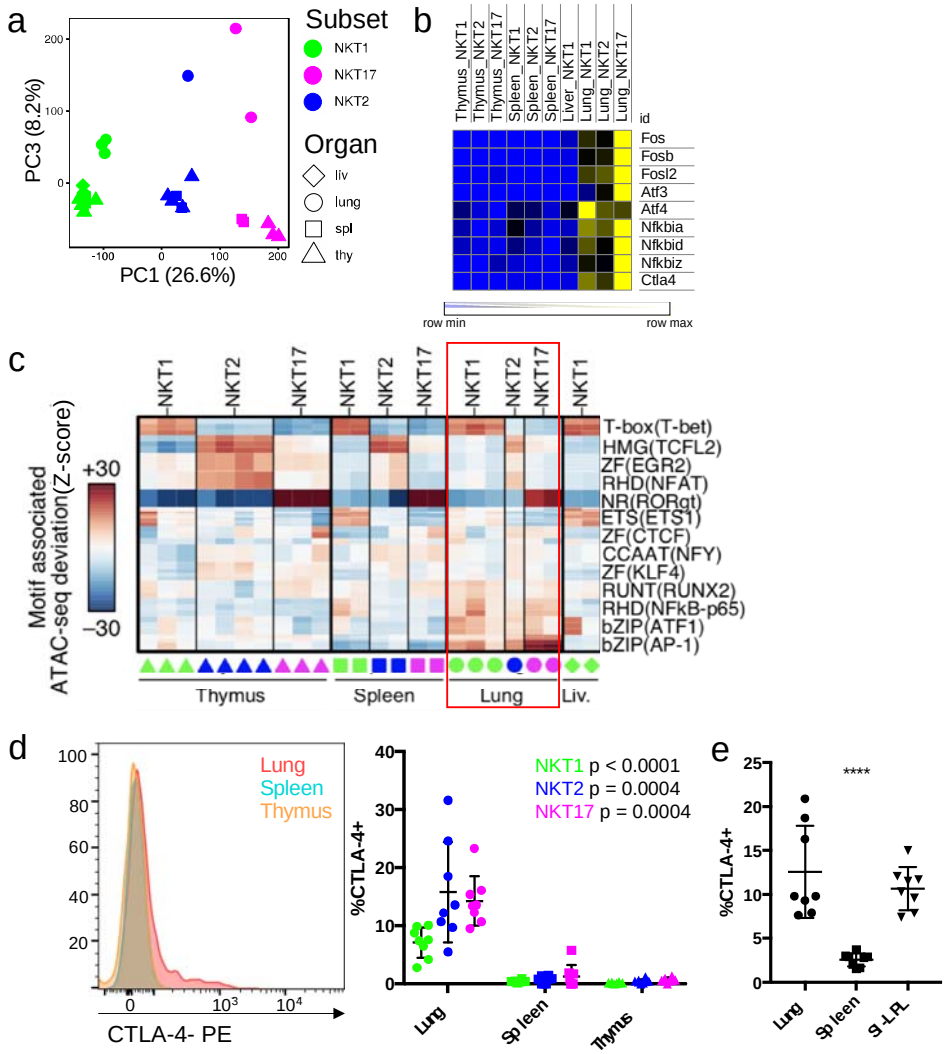

885

886 **Fig. 3. Lung-specific transcriptome and epigenome.** a. PC1 by PC3 display of
887 ATAC-seq data showing distribution of iNKT cell subsets from different tissues. b. Heat
888 map of relative RNA expression of selected AP-1 and ATF family genes in iNKT subsets
889 from the indicated sites. c. chromVAR computed deviation in ATAC-seq signal (Z-score)
890 at regions containing indicated transcription factor motifs. Motifs with a p-value less than
891 1e-25 are shown and families and representative members are labeled. Samples are
892 indicated at the bottom, iNKT cell subsets from the lung are boxed to highlight lung-
893 enriched motifs. d. Total CTLA-4 expression in permeabilized iNKT cells from the
894 indicated tissues. Representative cytogram of total iNKT cells (left) and percent CTLA-
895 4^+ cells within each subset from the different organs (right). Symbols depict individual
896 mice, error bars depict SD. Data are combined from five experiments, n = 8 mice,
897 statistical significance assessed via Kruskal-Wallis test. e. Total CTLA-4 expression in
898 permeabilized total iNKT cells from indicated tissues. Symbols depict individual mice,
899 error bars depict SD, n = 8 mice from two independent experiments. Statistical
900 significance assessed via one-way ANOVA.

bioRxiv preprint doi: https://doi.org/10.1101/2020.10.27.357673; this version posted October 27, 2020. The copyright holder for this preprint (which was not certified by peer review) is the author/funder. All rights reserved. No reuse allowed without permission.

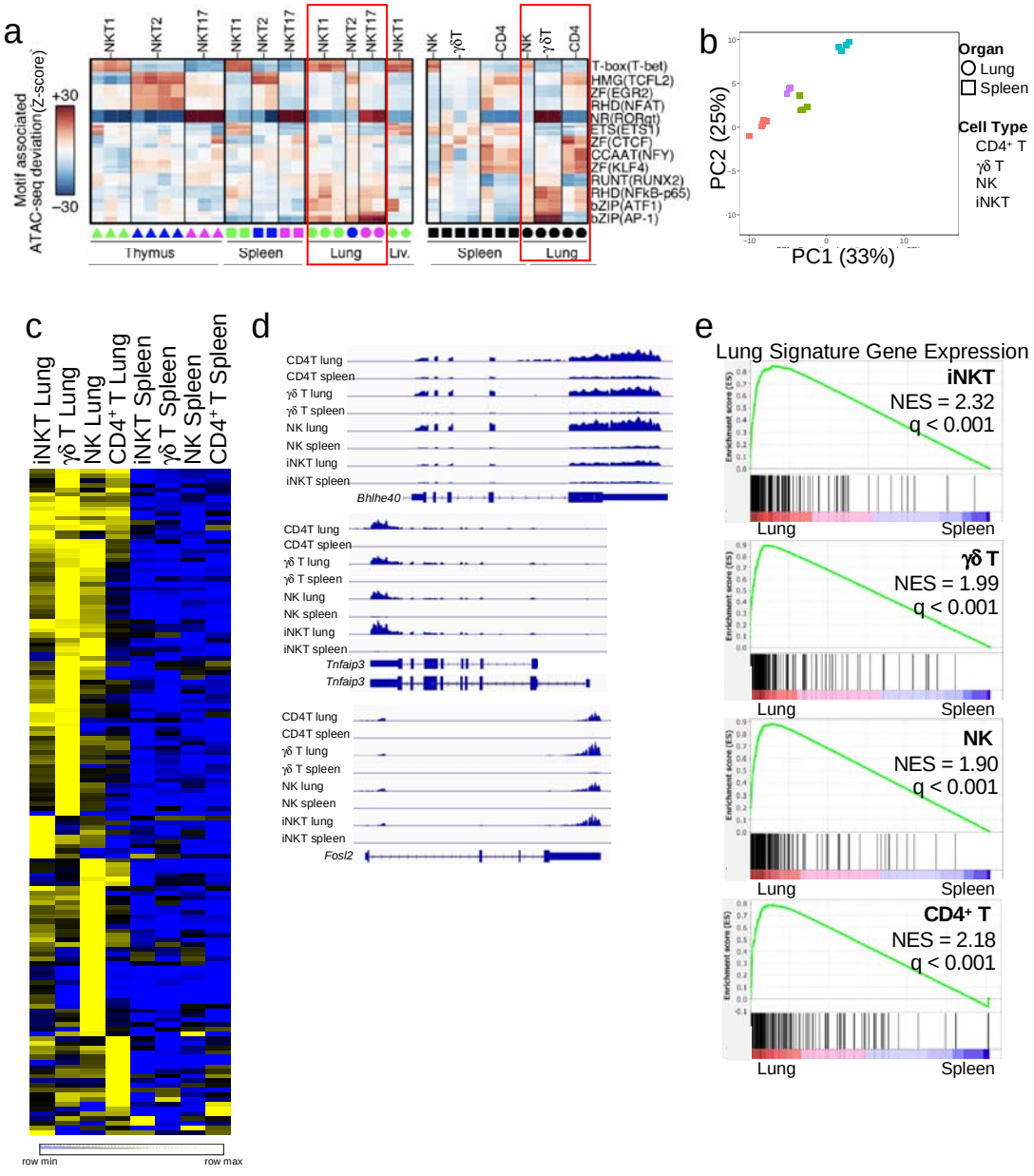

Fig. 4. Lung signature extends to other lung populations. a. chromVAR computed deviation in ATAC-seq signal (Z-score) at regions containing indicated transcription factor motifs between the indicated cell populations from spleen and lung. Motifs with a p-value less than 1e-25 are shown and families and representative members are labeled. Tissue source of the samples indicated at the bottom of the diagram; columns indicate number of replicates. b. PCA of RNA-seq data comparing lymphoid cell types isolated from lung and spleen. c. Heat map depicting the lung gene signature from Supplementary Fig. 3 with normalized transcript levels from RNA-seq data from the indicated cell types from lung and spleen. d. RNAseq read tracks in the *Bhlhe40*, *Tnfaip3* and *Fosl2* loci in samples from lung and spleen from indicated cell types. e. GSEA of pre-ranked comparisons of genes differentially expressed in lung iNKT cell subsets comparing each cell type within the lung to its counterpart in the spleen.

bioRxiv preprint doi: https://doi.org/10.1101/2020.10.27.357673; this version posted October 27, 2020. The copyright holder for this preprint (which was not certified by peer review) is the author/funder. All rights reserved. No reuse allowed without permission.

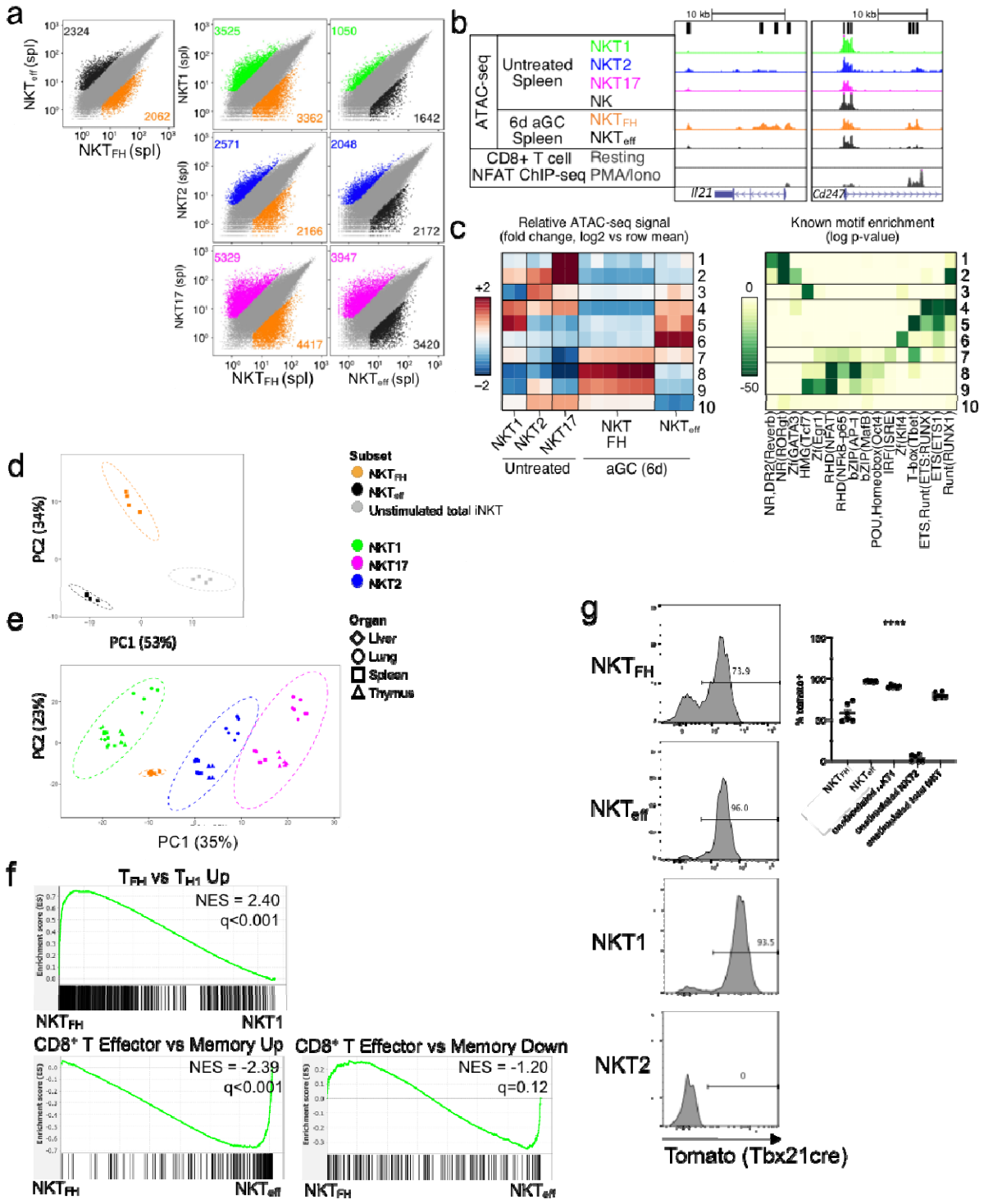

Fig. 5. Antigenic experience shapes the transcriptome and chromatin landscape of iNKT cells. iNKT cells from αGalCer-injected mice either selected for PD-1 and CXCR5 expression (NKT_{FH}) and or negative for both markers (NKT_{eff}) were sorted from the spleen of mice 6 days after injection (i.v.) with αGalCer. a. Scatterplots of mean ATAC-seq counts per peak comparing antigen experienced NKT_{FH} and NKT_{eff} (top left)

bioRxiv preprint doi: https://doi.org/10.1101/2020.10.27.357673; this version posted October 27, 2020. The copyright holder for this preprint (which was not certified by peer review) is the author/funder. All rights reserved. No reuse allowed without permission.

or pairwise comparisons of differentially accessible regions of chromatin for each of the sorted populations from antigen exposed mice compared to the corresponding subsets from unimmunized mice. Data from unimmunized mice are the same as depicted in Fig. 2. Colors indicate differentially accessible regions defined by limma/voom (details in Methods). b. ATAC-seq coverage (range of 0-600 for all samples) comparing the *Il21* and *Cd247* loci from unimmunized splenic iNKT cell subsets, splenic NK cells, and NKT_{FH} and NKT_{eff} from αGalCer-treated mice. NFAT ChIP-seq analysis of $CD8^+$ splenic T cells with and without PMA/ionomycin stimulation included for comparison[54]. c. Left, *k*-means clustering of relative ATAC-seq density (counts per million mapped reads/kb, log_2 fold change from the mean) identifies ten groups of accessible regions that vary similarly (rows), 2 sets for splenic NKT1, 2 for splenic NKT2, 2 for splenic NKT17, 6 for NKT_{FH} and 3 for NKT_{eff}. Columns indicate number of replicates. Right, motifs enriched in clusters of accessible regions. All motifs with a HOMER log p-value less than –15 and found in 10% or more regions in at least one cluster are shown. d. PCA analysis of RNA-seq data comparing NKT_{FH} to NKT_{eff} from αGalCer-immunized mice as well as to total iNKT cells from unimmunized mice. e. PCA analyses of RNA-seq data comparing splenic NKT1, NKT2 or NKT17 samples to spleen NKT_{FH} cells. f. Top: Plot of the distribution of genes upregulated in mainstream GC T_{FH} vs T_{H1} in a list of genes ranked by relative expression (directional p value) in NKT_{FH} vs splenic NKT1 cells using GSEA. Bottom (left and right): Plots of genes differentially regulated between $CD8^+$ effector vs memory against a directional p-ranked file comparing αGalCer-stimulated NKT_{FH} vs NKT_{eff}. Normalized Enrichment Scores (NES) and q values were determined by the pre-ranked GSEA algorithm. g. Expression of reporter in T-bet fate-mapping mice by NKT_{FH} and NKT_{eff} cells 6 days-post antigen exposure, and NKT1 and NKT2 cells and total iNKT cells from unstimulated mice; n = 6 mice per group, error bars depict SEM. Quantification on right, statistical significance assessed via Kruskal-Wallis test.

bioRxiv preprint doi: https://doi.org/10.1101/2020.10.27.357673; this version posted October 27, 2020. The copyright holder for this preprint (which was not certified by peer review) is the author/funder. All rights reserved. No reuse allowed without permission.

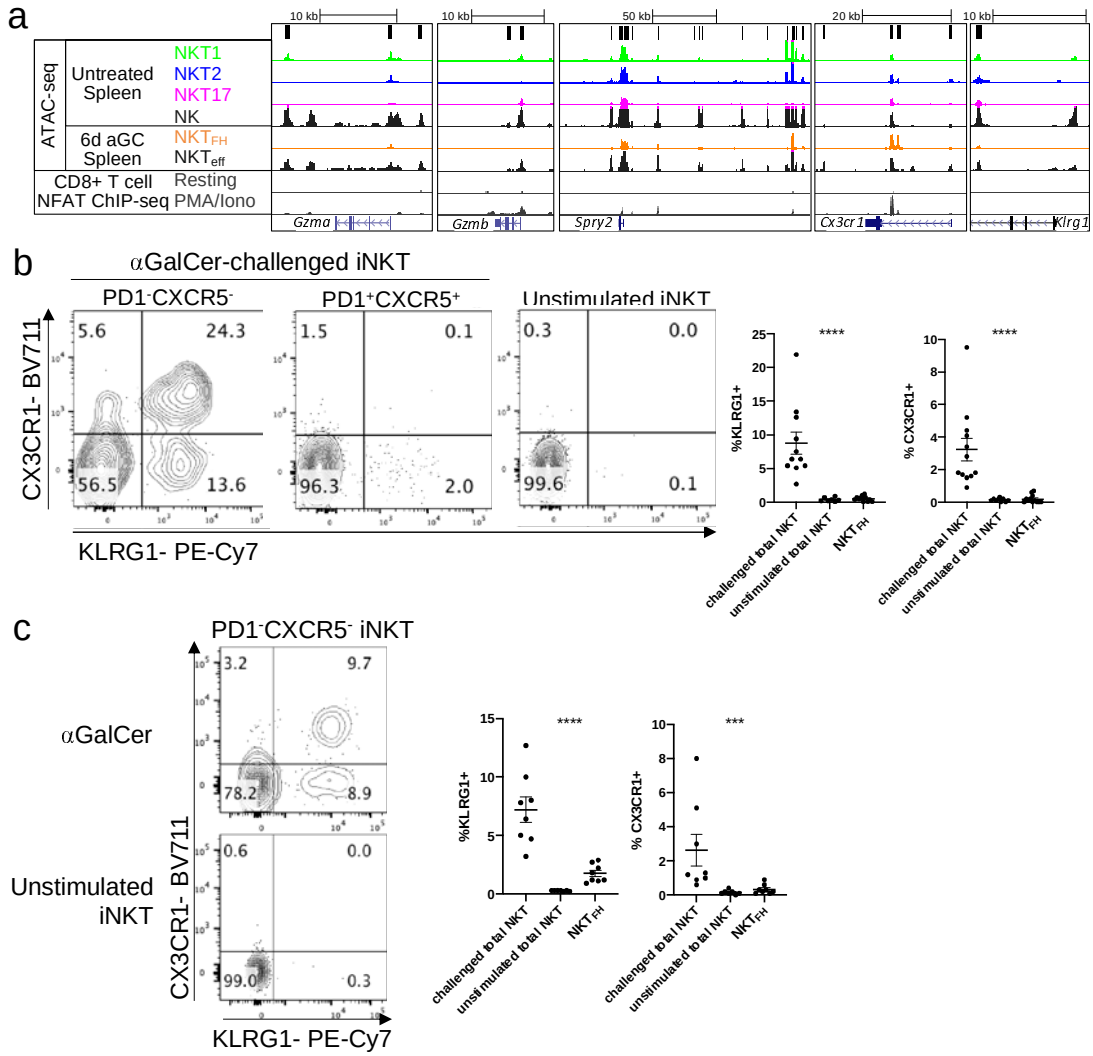

Fig. 6. Enhanced effector or NK cell signature in antigen-exposed iNKT cells. a. ATAC-seq coverage (with a range of 0-600 for all samples) at the *Gzma*, *Gzmb* and *Spry2* loci comparing untreated splenic iNKT cells subsets, spleen NK cells, NKT_{FH} and NKT_{eff} from mice injected 6 days earlier with αGalCer. NFAT1 ChIP-seq analysis of $CD8^+$ T cells with and without PMA/ionomycin stimulation included for comparison[54]. b. Flow cytometry analysis of expression of KLRG1 and CX3CR1 by the indicated populations of gated spleen iNKT cells at day 6 after antigen. Quantification on right, n = 11 mice (αGalCer challenged, KLRG1), n = 12 mice (αGalCer challenged, CXCR3), n = 6 mice (unstimulated, KLRG1), n = 8 mice (unstimulated, CXCR3), n = 11-12 mice (NKT_{FH}). c. Representative flow cytometry analysis of expression of NKT_{eff} markers CX3CR1 and KLRG1 by gated spleen PD-1^- $KLRG1^-$ iNKT cells at day 30 or later after antigen administration. Quantification of iNKT cells expressing NKT_{eff} markers, challenged mice analyzed at day 30 or later on right, n = 8 mice (αGalCer challenged, NKT_{FH}), n = 7 mice (unstimulated). b,c. Representative data from 3-5 experiments, error bars depict SEM, statistical significance assessed via Kruskal-Wallis test.